IEEE Journal of Microwaves

Received 15 November 2022; revised 2 March 2023 and 23 March 2023; accepted 24 March 2023. Date of publication 29 May 2023; date of current version 7 July 2023.

Digital Object Identifier 10.1109/JMW.2023.3263194

A Novel Analysis of Periodic Structures Based on Loaded Transmission Lines

ALBERTO MEDINA-RULL (Student Member, IEEE), FRANCISCO PASADAS, ENRIQUE G. MARIN, ANDRÉS GODOY, AND FRANCISCO G. RUIZ (Member, IEEE)

(Regular Paper)

[1]Pervasive Electronics Advanced Research Laboratory (PEARL), Departamento de Electrónica y Tecnología de Computadores, Facultad de Ciencias, Universidad de Granada, 18071 Granada, Spain

CORRESPONDING AUTHOR: Alberto Medina-Rull (e-mail: amrull@ugr.es).

The work of A. Medina-Rull was supported by MCIN/AEI/PTA grant, under Reference PTA2020-018250-I. The work of F. Pasadas was supported in part by PAIDI 2020 and the European Social Fund Operational Programme 2014-2020 under Grant 20804, and in part by the Ministerio de Universidades under Grant CAS21/00483. This work was supported in part by the FEDER/Junta de Andalucía-Consejería de Transformación Económica, Industria, Conocimiento y Universidades under Grants A-TIC-646-UGR20, B-RNM-375-UGR18, P20_00633, and MCIN/AEI/10.13039/501100011033, and in part by the European Union "NextGenerationEU"/PRTR under Grants PID2020-116518GB-I00, TED2021-129769B-I00, and TED2021-129938B-I00.

ABSTRACT Periodically loaded transmission lines are characterized by a frequency response with regular pass and stopbands. Interestingly, each of the passbands exhibits a peculiar comb-alike behavior, in which again, nested (or internal) pass and stopbands can be identified. In this work, we focus our attention on the effect that changing the characteristics of the periodic load (which is a varactor capacitance in our case) has in this peculiar response of the structure, providing a novel and detailed analysis of such bands. The control of the response of the structure when changing the properties of the load allows to adjust the transmission characteristics of the circuit once it is fabricated. To this purpose, we derive the design equations of the periodically loaded structures, obtaining the expressions which govern the position and number of the transmission peaks, i.e., the points where $|S_{21}| = 1$ for both cases, the frequency sweep and the capacitance sweep. We experimentally validate our analysis by fabricating a periodic structure with five unit cells and compare the measurements against both theoretical results and circuit simulations to an excellent agreement. The present analysis paves the way towards further exploitation of these kind of structures for the design of different microwave applications such as tunable filters or phase shifters.

INDEX TERMS Capacitive loading, circuit analysis, periodic structures, RF circuits, transmission lines.

I. INTRODUCTION

Periodic structures are recurrent in physics, ranging from electronics to quantum mechanics, passing by material science and semiconductor crystal theory [1], [2], [3]. In the particular realm of microwave engineering, periodically loaded transmission lines are well known and have been widely exploited as filters [4], [5], [6], [7] and phase shifting devices [8], [9], [10], [11], [12]. The latter application has been recently addressed by the employment of complex structures, enabling the improvement of the phase shift range while, simultaneously, increasing the return losses [13], [14], [15].

Being a long-established topic in microwave engineering, the analysis of periodic transmission line structures has led to different treatments. The most general and well-known study focuses on the necessary conditions for a wave to propagate without attenuation through an infinite periodic structure, formed by repeated unit cells such as the one shown in Fig. 1 (see, for example, [4] and [5] and the references therein). The unit cell of this periodic structure, comprises two segments of a transmission line (TL) and a shunt susceptance in between. The condition for the wave to propagate unattenuated is that the voltage (V_n) and current (I_n) at some point n of the periodic structure must equal the voltage (V_{n+1}) and current (I_{n+1}) at the point $n + 1$, except for a phase shift difference due to the propagation delay from point n to $n + 1$. This delay is related to the propagation constant of the periodically loaded TL,

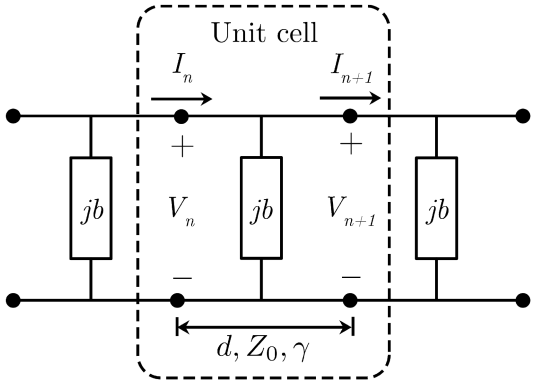

FIGURE 1. Periodic structure unit cell. V_n and I_n are the voltage and current at port n, respectively. d, Z_0 and γ are the total length, characteristic impedance and propagation constant of the TLs conforming the unit cell, respectively. b is the susceptance of the shunt admittance.

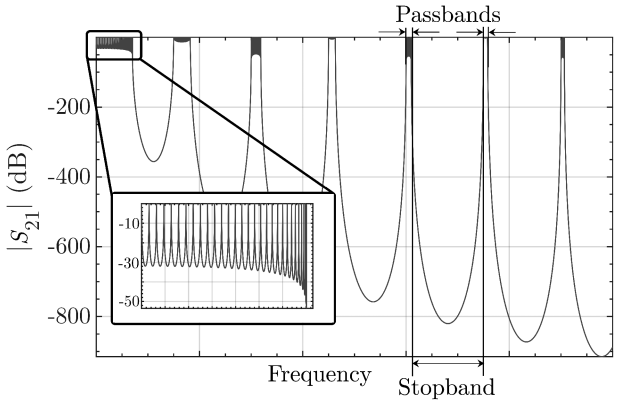

FIGURE 2. Characteristic frequency response of the periodic structure of Fig. 1 for a very large number of unit cells. The inset shows a zoom of one of the passbands.

$\gamma = \alpha + j\beta$, where α is the attenuation constant and β the phase constant. If $\alpha = 0$ and $\beta \neq 0$, the wave is not attenuated through the line, delimiting the so-called passbands of the structure. In contrast, when $\alpha \neq 0$ and $\beta = 0$, the wave is attenuated during its propagation, giving rise to the so-called stopbands (see Fig. 2).

This remarkable frequency response reveals itself more striking when looking in more detail at the passbands, which exhibit a comb-alike shape, yielding to new pass and stopbands very close to one another (see Fig. 2 inset). Moreover, this peculiar ripple is also observed when sweeping the susceptance (b), meaning that the use of a variable capacitor would enable the possibility of changing from one band to another. In fact, even though these nested passbands/stopbands are not as highly differentiated in magnitude as the main ones, the considerably smaller spacement between two consecutive bands is a distinguishing advantage with great potential for a number of microwave applications, such as tunable filters or phase shifters. To bring this potential to practice, it becomes essential to know the position of the transmission peaks, i.e., the points where the available power is transmitted to the load. However, in spite of the simplicity and relevance of the analysis, it has been historically obliterated and concealed from practical microwave applications, mostly motivated by the twofold intrinsic limitations of the generic analysis [4], [5]: (i) it is based on an infinite periodic structure, and (ii) it considers only two alternatives for the wave in the structure: either it does propagate or not, meaning that it is not possible to account for the ripple inside each passband.

In the case of the analysis of a finite periodic structure, it is worth to mention a few works shedding light on the topic. In [16], an analysis of the input impedance of cascaded identical twoport networks was addressed, concluding that its value approached one of the iterative impedances of the twoports no matter what termination was used. In a specific case of the study it was observed that the input impedance was cyclic, meaning that for a certain number of unit cells n, the input impedance was the same as for $2n, 3n, 4n, \ldots$. In [17], an alternative analysis was presented based on second-degree difference equations for the current along a cascade network. One of the examples provided to illustrate the analysis consisted of uniform networks with symmetrical passive sections, similar to the unit cell shown in Fig. 1 but slightly modified, substituting each TL section by an inductor. The analysis developed by means of this methodology resulted in the observation of the ripple inside the main passband, yet no exact method was provided to calculate the transmission peaks of this ripple.

Both references were, indeed, indebted to the original theory developed in [18] for the cascading of matrices and its use to calculate the transmission and reflection coefficients of a periodic structure. Also based on this theory, almost three decades later another investigation experimentally observed the ripple and proposed a theoretical analysis to rationalize the measurements [19], but still no exact expression was specified so as to calculate the transmission peaks nor to enable the design of the structure. Nonetheless, some relevant findings resulted, being the most remarkable one that the number of transmission peaks inside the first passband is $N = n - 1$, with n the number of cascaded unit cells.

Among all these studies, the work by Griffiths and Steinke [20] stands out, which presents a thorough and complete analysis of wave propagation in one-dimensional periodic structures within different media, ranging from quantum mechanics to optical media, giving equations to calculate the transmission characteristics of finite periodic structures with any arbitrary number of unit cells.

Despite the interest of these pioneering works, there are still many relevant aspects about the periodic structures to be unveiled in order to take full advantage of the possibilities that they provide. Specifically, only the frequency response of the structures has been considered in the previous analysis, but none of them explores the impact of changing the properties

of the loading element, like the capacitance in the case of a capacitive loading, which could be of great utility as it could be used to tune the circuit response once it is fabricated and by keeping the operating frequency. In addition, none of the previous analyses presents explicit expressions to determine the position of the transmission peaks of the ripple inside the main passbands.

To the purpose of giving a response to these questions, this work proposes a novel and comprehensive analysis based on S-parameters of periodic structures formed by TLs periodically loaded able to determine the position of the transmission peaks when sweeping the frequency of the input signal (frequency response) and, specially, when changing the properties of the loading (the capacitance in our case). One of the main outcomes of this analysis is a set of equations that can be used to gain control of both, the frequency response of the structure and its dependence with parameters such as the susceptance (b) or the characteristic impedance of the TLs (Z_0). This set of equations provides all the information regarding the particular response of the structure, giving the possibility of exploiting it in a large number of microwave applications. For instance, tunable filters, phase shifters, or reconfigurable matching networks could be exploited with the analysis of the structures presented. Our theory is experimentally tested by the fabrication of a demonstrator circuit with five unit cells, whose behavior is compared against both circuit simulations and the here-developed theory, achieving an excellent agreement.

II. ANALYSIS

We start by defining the transmission matrix ($\boldsymbol{T}$) of the unit cell in Fig. 1. Assuming lossless TL sections (i.e., $\alpha = 0$), we can write:

$$\boldsymbol{T} = \begin{bmatrix} \left(1+\frac{y}{2}\right)e^{j\beta d} & -\frac{y}{2} \\ -\frac{y}{2} & \left(1-\frac{y}{2}\right)e^{-j\beta d} \end{bmatrix} \tag{1}$$

where $y = Y/Y_0$ is the admittance of the shunt element (Y) normalized to the characteristic admittance of the TL sections (Y_0); β is the phase constant of the TL, and d is the physical length of the TL sections of each unit cell. In a periodic structure with n identical unit cells, the T-matrix of the cascade can be evaluated as $\boldsymbol{T}^n$, where the n-th power of the T-matrix can be written as [18]:

$$\boldsymbol{T}^n = U_{n-1}(\nu)\boldsymbol{T} - U_{n-2}(\nu)\boldsymbol{I} \tag{2}$$

with U_n the second kind Tschebysheff polynomial of order n, $\boldsymbol{I}$ the identity matrix and ν:

$$\nu = \frac{T_{11}+T_{22}}{2} \tag{3}$$

where T_{ij} stands for the (i, j) element of $\boldsymbol{T}$. Assuming that the shunt admittance of the unit cell of Fig. 1 is purely imaginary, $y = jb$, ν can be obtained using (3) and (1) as:

$$\nu = \cos(\beta d) - \frac{b}{2}\sin(\beta d) \tag{4}$$

so that $\nu \in \mathbb{R}$.

Thus, the T-matrix of a periodic structure formed by the concatenation of n unit cells can be written as:

$$\begin{aligned} \boldsymbol{T}^n &= \begin{bmatrix} T_{11,n} & T_{12,n} \\ T_{21,n} & T_{22,n} \end{bmatrix} \\ &= \begin{bmatrix} U_{n-1}T_{11} - U_{n-2} & U_{n-1}T_{12} \\ U_{n-1}T_{21} & U_{n-1}T_{22} - U_{n-2} \end{bmatrix} \end{aligned} \tag{5}$$

where we have introduced the notation $T_{ij,n}$ for the (i, j) matrix element of $\boldsymbol{T}^n$. The conversion matrix between T and S-parameters [5] enables the evaluation of the periodic structure performance in terms of its S-parameters:

$$\begin{aligned} \boldsymbol{S}_n &= \begin{bmatrix} S_{11,n} & S_{12,n} \\ S_{21,n} & S_{22,n} \end{bmatrix} \\ &= \begin{bmatrix} \frac{T_{21,n}}{T_{11,n}} & \frac{T_{11,n}T_{22,n}-T_{12,n}T_{21,n}}{T_{11,n}} \\ \frac{1}{T_{11,n}} & -\frac{T_{12,n}}{T_{11,n}} \end{bmatrix} \end{aligned} \tag{6}$$

It is worth to note that $\boldsymbol{S}_n$ is the S-matrix of the whole periodic structure with n sections, and $S_{ij,n}$ its corresponding (i, j) element.

Then, in order to find the transmission peaks, i.e. the points where the whole available power is transmitted from the input to the output, it is necessary to impose $|S_{21,n}| = 1$. From (6), this can be achieved if and only if $|T_{11,n}| = 1$, or equivalently $|U_{n-1}T_{11} - U_{n-2}| = 1$. However, the complexity of this expression for almost any concatenation of unit cells makes it unfeasible to evaluate it analytically (see Appendix A).

However, a lossless passive linear network as the one in Fig. 1 complies with the condition $|S_{21,n}| = 1 \Leftrightarrow |S_{11,n}| = 0$. From (6), $S_{11,n} = T_{21,n}/T_{11,n}$, so that $|T_{21,n}| = 0$ is the only way of accomplishing $|S_{11,n}| = 0$. Thus the transmission peaks satisfy:

$$|T_{21,n}| = |U_{n-1}T_{21}| = 0 \tag{7}$$

whose solutions imply: (i) $|T_{21}| = 0 \Leftrightarrow b = 0$, i.e. the susceptance is zero which is discarded as it is a non practical case; (ii) $|U_{n-1}(\nu)| = 0$, i.e. the zeros of the Tschebysheff polynomial of order $n-1$, whose position is determined as [21]:

$$\nu_k^{n-1} = \cos\left(\frac{\pi k}{n}\right) \tag{8}$$

with ν_k^{n-1} denoting the k-th zero of the second kind Tschebysheff polynomial of order $n-1$, and $k = [1, n-1]$ with $k \in \mathbb{Z}$. Thus, for a periodic structure based on a lossless passive linear network with n unit cells, $|S_{11,n}| = 0$ and $|S_{21,n}| = 1$ if and only if $|U_{n-1}(\nu)| = 0$, i.e. for $\nu = \nu_k^{n-1}$ as defined by (8) (see Appendix B for a thorougher analysis). The number of transmission peaks for n unit cells is $N = n-1$, in addition to the zero produced by the case $b = 0$, as it was indeed experimentally observed in [19].

We can thus determine the conditions that are fulfilled at the transmission peaks by relating (4) and (8):

$$v_k^{n-1} = \cos(\beta d) - \frac{b}{2}\sin(\beta d) = \cos\left(\frac{\pi k}{n}\right) \tag{9}$$

Solving (9) for b we obtain:

$$b_k = \frac{2}{\sin(\beta d)}\left[\cos(\beta d) - \cos\left(\frac{\pi k}{n}\right)\right] \tag{10}$$

where the notation b_k is introduced for the k-th solution of the equation.

Equation (10) provides an explicit expression to calculate the values of b_k that correspond to the transmission peaks ($|S_{21,n}| = 1$ and $|S_{11,n}| = 0$) of the lossless periodic structure. In other words, the proposed expression constitutes the design equation for a periodic structure with an arbitrary number n of unit cells, and determines the conditions for the optimum transmission peaks in terms of the different parameters of the unit cell (e.g. TL length and susceptance). It is worth to note that while changing the structure of the unit cell will modify v, the design equations are general for any unit cell (provided it is lossless, passive and linear) and can thus be exploited by straightforwardly recalculating v of the new unit cell and using it in (9).

III. SYSTEM DESIGN AND FABRICATION

A. INDUCTIVE OR CAPACITIVE SUSCEPTANCE, b

Equation (10) allows both positive- and negative-valued solutions of b_k, which correspond to a capacitive or inductive-like susceptance, respectively. For our design, we have opted for a physical implementation of the periodic TL based on a variable capacitor, and have then to analyze under which particular circumstances would b_k be positive. Assuming that the length of each TL section will be lower than $\lambda/4$, then $\beta d \leq \pi/2$, making $\cos(\beta d)$ and $\sin(\beta d)$ non-negative. Under this assumption, b_k will be positive when the following relation is accomplished:

$$\cos\left(\frac{\pi k}{n}\right) < \cos(\beta d) \tag{11}$$

Since in the first quadrant ($\beta d < \pi/2$) the cosine is a monotonically decreasing function, (11) implies:

$$\beta d < \frac{\pi k}{n} \Leftrightarrow d < \frac{k}{2n}\lambda \tag{12}$$

From (12) it can be concluded that the most restrictive situation occurs for $k = 1$; in this case, the condition to guarantee $b > 0$ and thus that the susceptance corresponds to a varactor reads as:

$$d < \frac{\lambda}{2n} \tag{13}$$

In other words, the total number of unit cells of the periodic structure sets a limit for the length of the TLs of each unit cell in order to make all b_k values positive. To gain further insight, we have simulated a periodic structure as the one in Fig. 1 with $n = 5$ and $f = 3$ GHz, making use of the commercial circuit simulator Advanced Design System (ADS^{TM}) [22]. For this particular case, (13) imposes the limit $d < \lambda/10$. Fig. 3 shows the simulation results in terms of the $|S_{11}|$ parameter for different values of the electrical length, $d = \lambda/4$, $\lambda/8$, $\lambda/12$. It can be observed that, according to (13), the case that satisfies $d < \lambda/10$ shows the four expected zeros for positive values of b. Although physically meaningless, $b = 0$ is always a zero as discussed in (7).

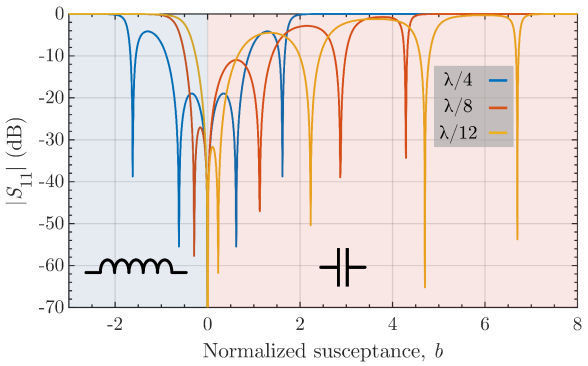

FIGURE 3. $|S_{11}|$ (dB) parameter of a periodic structure with $n = 5$ versus the normalized susceptance of the periodic loading, b, for different values of the electrical length of the TL sections: $\lambda/4$, $\lambda/8$, $\lambda/12$. Only when $d = \lambda/12$ (i.e., $d < \lambda/10$) the four expected zeros, b_k, are positive.

B. FULLY LOCATING THE TRANSMISSION PEAKS

Once the susceptance $b > 0$ is physically realized in the form of a variable capacitor, i.e., $b = Z_0\omega C$, with $\omega = 2\pi f$, the value of b depends on the capacitance of the varactor and on the frequency. Even though both entail a proportional change on b, sweeping f does not only change b, but it concomitantly modifies the electrical length of the TLs. As a consequence, changing f will not produce the same result as changing C, and the frequency position of the transmission peaks, corresponding to the zeros of $|S_{11}|$ in Fig. 3, cannot be directly inferred from the values of b.

In order to predict these frequency zeros, from (9) we can write:

$$\cos\left(\frac{2\pi d}{v_p}f\right) - Z_0\pi f C \sin\left(\frac{2\pi d}{v_p}f\right) = \cos\left(\frac{\pi k}{n}\right) \tag{14}$$

where v_p is the propagation speed: $v_p = c/\sqrt{\epsilon_{\text{eff}}}$; and ϵ_{eff} is the effective dielectric constant of the media. Equation (14) can be indeed solved to obtain both, the frequency and the capacitance transmission peaks by fixing either the capacitance or the frequency, respectively.

In addition to the simulation, (14) has been solved for f (fixing C_{var}) and for C_{var} (fixing f) in order to reveal the theoretical frequency and capacitance positions of the zeros of the structure. The results, depicted as vertical lines in Fig. 4, coincide with the simulated zeros of $|S_{11}|$, demonstrating the ability of (14) to predict the position of the zeros as much when changing f as when changing b. Equation (14) can be thus deemed as the main design equation of the structures.

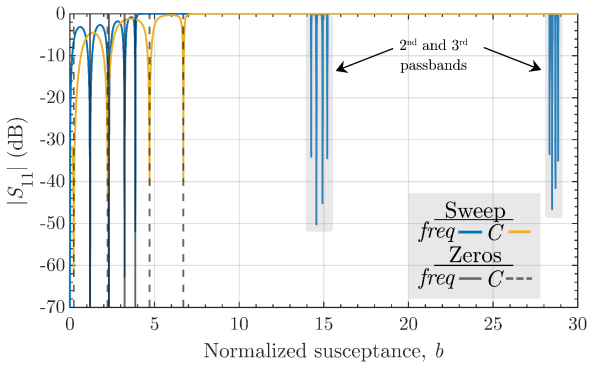

FIGURE 4. Simulated $|S_{11}|$ (dB) as a function of b, for a periodic structure with $n = 5$ and $d = \lambda/12 = 8.3$ mm at $f = 3$ GHz, considering $v_p = c$. A frequency sweep with constant capacitance $C_{var} = 2.5$ pF (blue line) and a capacitance sweep with constant frequency $f = 3$ GHz (yellow line) have been considered. Vertical lines correspond to theoretical values for the zeros of the $|S_{11}|$ obtained from (14). The zeros on the second and third passbands on the frequency sweep are not shown due to visualization purposes.

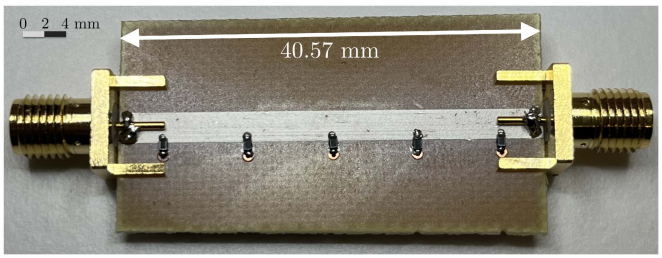

FIGURE 5. Fabricated periodic structure with $n = 5$ in microstrip technology.

C. FABRICATION AND MEASUREMENT SETUP

To experimentally validate the previous design, a periodic structure with five unit cells ($n = 5$) has been fabricated (Fig. 5) in microstrip technology, using a FR4 substrate fabricated by C.I.F.™ [23] with a dielectric constant of $\epsilon_r = 4.7$ and a dielectric thickness of $H = 1.6$ mm, where the back conductor is made of copper while the top conductor is made of a curated conductive silver ink fabricated by Voltera™ with a resistivity of 1.27x 10^{-7} Ω m [24]. For the vias, copper rivets have been used, while the Infineon™ BBY55-02 V is used as the variable capacitor [25]. For input and output connections, two SMA connectors have been welded to the input and output ports of the structure.

The measurement setup consists of the Keysight™ ENA 5061B and two ZFBT-4R2GW-FT+ Mini-Circuits™ bias tees. For the DC bias, the DC output of the ENA was used. The overall measurement setup is shown in Fig. 6(a). Besides, the Impedance Analyzer Keysight™ E4990 A, with the SMD component test fixture Keysight™ 16034E (Fig. 6(b)), was used to characterize the C-V_R curve of the commercial varactors up to a maximum frequency of 40 MHz, with V_R being the reverse voltage applied.

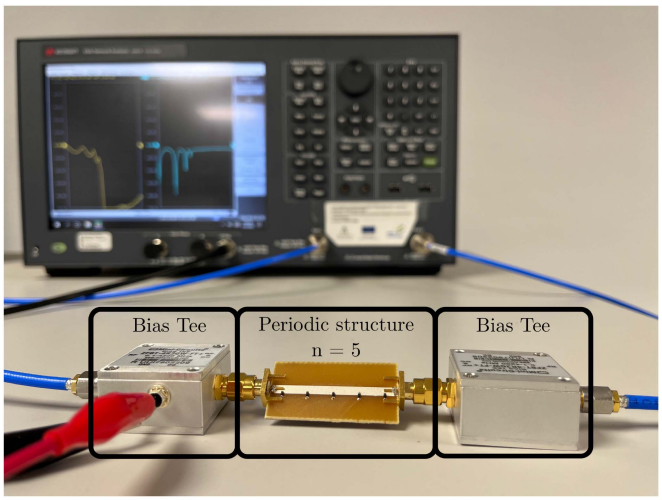

(a)

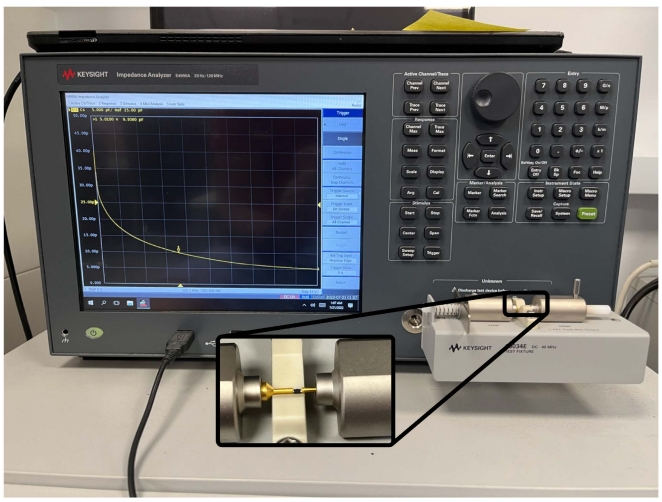

(b)

FIGURE 6. (a) Keysight™ ENA 5061B and additional circuitry employed for prototype RF measurements, and (b) Keysight™ E4990 A impedance analyzer along with the SMD component fixture Keysight™ 16034E for SMD component characterization.

IV. RESULTS

The system designed and fabricated in this work, i.e. a microwave periodic structure formed by loaded TLs, relies in microstrip technology and SMD commercial varactors, what demands to carefully characterize the eventual parasitics that could affect the intrinsic behavior of the circuit, specially at high frequencies. This limitation of the employed technology is not intrinsic to the here proposed theoretical analysis and design procedure, which could be fairly exploited in integrated circuit (IC) technology, but becomes relevant in the present implementation at high frequencies.

In particular, we identify two main extrinsic effects that must be de-embedded for a fair comparison with the theory. The first one is produced by the parasitic elements inherent to the commercial varactors. Due to the packaging, some parasitic series and/or shunt elements need to be considered

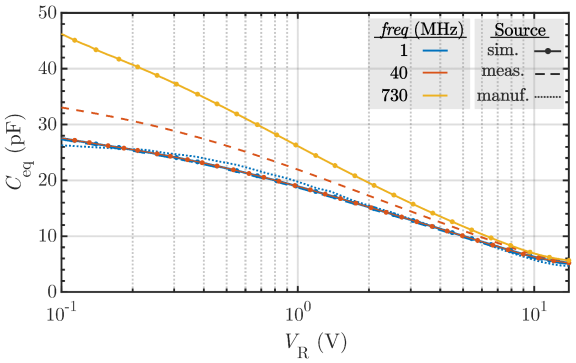

FIGURE 7. BBY55-02 V variable capacitor characterization. The measurements performed with the impedance analyzer are represented by dashed lines; with solid lines, the simulation results are shown; and the dotted curve is the one provided by the manufacturer.

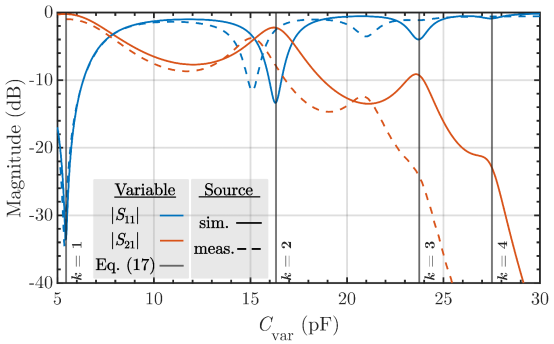

FIGURE 8. $|S_{11}|$ and $|S_{21}|$ (dBs) as a function of the capacitance of the varactors (C_{var}), for a frequency value of 730 MHz. A voltage sweep from 0 to 14 V is performed. The solid lines represent the circuit simulation results, the dashed lines represent the experimental measurements. The vertical lines correspond to the theoretically calculated values for the transmission peaks.

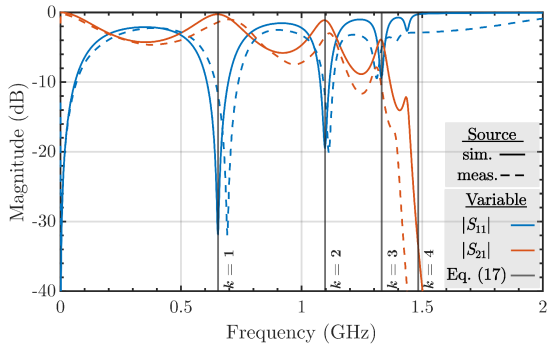

FIGURE 9. $|S_{11}|$ and $|S_{21}|$ (dBs) as a function of the frequency for a reverse bias of $V_R = 10$ V, that corresponds with a $C_{var} = 7$ pF. The solid lines represent the simulation results, and the dashed lines represent the experimental measurements. The vertical lines correspond to the theoretically calculated values for the transmission peaks.

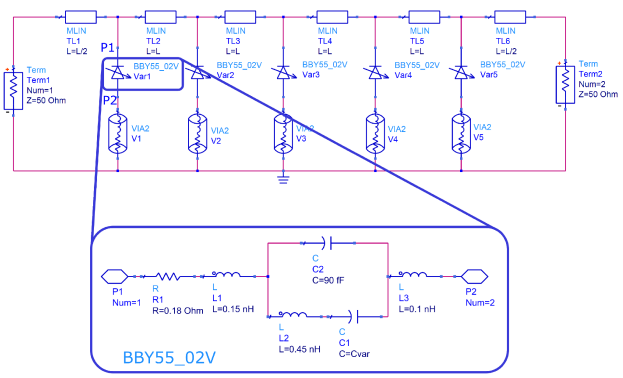

FIGURE 10. Simulation schematic of the periodic structure considering the parasitic elements and the ground vias. Inset: BBY55-02 V equivalent circuit showing the parasitic elements provided by the manufacturer.

in the form of extrinsic inductors, resistors or capacitors for a proper modeling of the actual varactor. Even though these parasitic elements are commonly disregarded, their effect — particularly at high frequencies — is not negligible, as will be evinced later. The second extrinsic effect has its origin on the ground vias. In microstrip technology, grounding is usually achieved by connecting the top and bottom sides of the printed circuit board (PCB) with conductive vias. These vias, whose length equals the thickness of the board, add a section of TL whose electrical length cannot be neglected as the frequency increases.

Due to these parasitics, the impedance of the varactors changes and so does their capacitance. In order to assess this effect and at the same time to characterize the varactors, in Fig. 7 the equivalent varactor capacitance (C_{eq}) versus V_R curves obtained from three different sources are shown: (i) from the manufacturer datasheet at 1 MHz (blue dotted line), (ii) from the experimental measurements carried out with the impendance analyzer at 1 MHz and 40 MHz (blue and red dashed lines, respectively) and (iii) from circuit simulations performed with ADS^{TM} of the equivalent circuit that includes the parasitics provided by the manufacturer, shown in the inset of Fig. 10, at 1 MHz, 40 MHz and 730 MHz (blue, red and yellow solid lines, respectively). Two conclusions can be extracted from this Figure: (i) as frequency increases, the equivalent capacitance of the varactors (C_{eq}) is higher than their reported variable capacitance (C_{var}), which highlights the crucial role that the parasitics play as frequency increases, and only at low frequencies $C_{eq} = C_{var}$; and (ii) the packaging parasitics provided by the manufacturer do not match the measured ones, as can be seen at the $f = 40$ MHz curve, where the measured equivalent capacitance is higher than the simulated one (which is still very close to the 1 MHz curves). This mismatch increases as the applied reverse voltage is reduced (i.e., as C_{var} is bigger). So as to account for the effects of the parasitics and with the aim of making the comparison between measurements and simulations fair, a de-embedding procedure that allows for the transformation of the equivalent capacitance C_{eq} to the actual varactor capacitance C_{var} is implemented by using:

$$C_{var} = \frac{C_2 - C_{eq} + C_2 C_{eq}(L_1 + L_3)\omega^2}{\omega^2[C_2 L_2 - C_{eq} L_t + C_2 C_{eq} L_2 (L_1 + L_3)\omega^2] - 1} \quad (15)$$

where $L_t = L_1 + L_2 + L_3$, and the elements L_1, L_2, L_3, C_{var} and C_2 are shown in the inset of Fig. 10, and their values were provided by the manufacturer [26]. Hence, due to their above mentioned underestimation, a certain deviation of the simulated with respect to the experimental data is expected, especially for low V_R (high C_{var}) and high f. A thorough discussion of the effects originated by the parasitics is carried out in Appendix C.

Now, we proceed to evaluate the goodness of the proposed theoretical analysis and system design by comparing (see Figs. 8 and 9): (i) the simulation of the periodic structure depicted in Fig. 10 making use of ADS^{TM} (solid lines), (ii) the experimental measurements of the circuit (dashed line), and (iii) the theoretical transmission peaks positions calculated with (14) (grey vertical lines). In particular, Fig. 8 shows $|S_{11}|$ and $|S_{21}|$ in decibels as a function of the varactor capacitance C_{var} for $f = 730$ MHz, which is the frequency that allows the exhibition of the four expected zeros when the voltage is swept from 0 to 14 V. Fig. 9 shows $|S_{11}|$ and $|S_{21}|$ in decibels as a function of the frequency for a reverse bias $V_R = 10$ V, that corresponds with a capacitance value of the varactors of $C_{var} = 7$ pF. As mentioned earlier, in Fig. 8 the x-axis has been de-embedded with the described process and, in addition to that, the effect of the vias connected to the ground has been accounted as much in the simulations, by using the ADS^{TM} element to that effect, as in the de-embedding, by following the same theoretical approach as in the ADS^{TM} element [27].

From Figs. 8 and 9 it can be highlighted the good agreement achieved between circuit simulation and experimental measurements as well as with the theoretically predicted transmission peaks. In particular, in Fig. 8, for $C_{var} < 12$ pF, the agreement is excellent. However, due to the analyzed underestimation of the parasitics, for $C_{var} > 12$ pF, the predicted behavior is shifted towards higher capacitive values. In contrast, in Fig. 9, for $C_{var} = 7$ pF the agreement is excellent as the frequency has a low impact on the equivalent capacitance for $C_{var} < 12$ pF, as Fig. 7 shows. Figs. 8 and 9 clearly show the $N = n - 1 = 4$ transmission peaks (in addition to the transmission peak at $b = 0$).

V. CONCLUSION

In this work we have presented a novel analysis of periodically loaded transmission lines that provides the explicit design equations to locate the transmission peaks originated by these structures, focusing on the response when changing the characteristics of the periodically loading element. These equations account for the physical and electrical characteristics of the unit cell, such as the electrical length, characteristic impedance, operating frequency or loading susceptance, and, importantly, the number of unit cells that form the system. We have validated the developed theory against both, simulations carried out with a commercial circuit simulator (ADS^{TM}), and experimental measurements of a fabricated prototype, achieving an excellent agreement. The achieved accurate control of such transmission peaks is planned to be exploited in the design of a variety of microwave applications such as phase shifters or tunable filters. Finally, though the microwave theory conceived in this work is expected to be applied in integrated circuit technology, the demonstrator is fabricated with SMD components, and therefore, the extrinsic contribution of parasitics due to the packaging of the varactors and the ground vias impacts on the circuit performance, mainly at high frequencies. These aspects can be nevertheless captured by our theoretical model by substituting the ideal susceptance by an equivalent one that includes the effect of all the extrinsic elements at high-frequency, evidencing that the theory here presented can be adapted to real scenarios where deviations from the ideal device behavior are expected.

APPENDIX A
CALCULATION OF $T_{11,n} = 1$

The transmission peaks in the passband ripple of the periodic structure satisfy the condition $|S_{21,n}| = 1$. From (6), this is achieved if and only if $|T_{11,n}| = 1$, or equivalently $|U_{n-1}T_{11} - U_{n-2}| = 1$. The resulting equation becomes impractical. In order to exemplify this assessment, we propose to address a periodic structure of $n = 3$ unit cells. We calculate $\boldsymbol{T}^3$ as:

$$\begin{aligned}\boldsymbol{T}^3 &= U_2(\nu)\boldsymbol{T} + U_1(\nu)\boldsymbol{I} \\ &= \begin{bmatrix} (4\nu^2-1)T_{11} - 2\nu & (4\nu^2-1)T_{12} \\ (4\nu^2-1)T_{21} & (4\nu^2-1)T_{22} - 2\nu \end{bmatrix}\end{aligned} \tag{16}$$

where $U_1(\nu)$ and $U_2(\nu)$ are determined by using (4) and the recursive formula $U_{n+1}(\nu) = 2\nu U_n(\nu) - U_{n-1}(\nu)$:

$$\begin{aligned}U_1(\nu) &= 2\left(\cos(\beta d) - \frac{b}{2}\sin(\beta d)\right) \\ U_2(\nu) &= 4\nu^2 - 1 = 4\left(\cos(\beta d) - \frac{b}{2}\sin(\beta d)\right)^2 - 1\end{aligned} \tag{17}$$

To calculate the $S_{21,3}$ parameter, we would need to evaluate $T_{11,3} = (4\nu^2 - 1)T_{11} - 2\nu$ and we would still have to calculate the inverse of the expression and further simplify it to be able to obtain the magnitude and argument of S_{21}. As abovementioned, even in this simple scenario with $n = 3$, the resulting solution is impractical.

APPENDIX B
PROPERTIES OF THE PERIODIC NETWORK AND THE TSCHEBYSHEFF POLYNOMIALS

From the properties of a passive linear microwave network (and assuming $T_{11,n}$ is finite and $T_{21,n} \neq 0$), we can observe that:

$$\begin{aligned}|U_{n-1}| = 0 \Leftrightarrow |T_{21,n}| = 0 \Leftrightarrow |S_{11,n}| = 0 \Leftrightarrow \\ \Leftrightarrow |S_{21,n}| = 1 \Leftrightarrow |T_{11,n}| = 1 \Leftrightarrow |U_{n-2}| = 1\end{aligned} \tag{18}$$

but indeed, a known property is that, at the zeros of the $n-1$ Tschebysheff polynomial, $|U_{n-1}(\nu = \nu_k^{n-1})| = 0$, the $n-2$ Tschebysheff polynomial satisfies $|U_{n-2}(\nu = \nu_k^{n-1})| = 1$ [21]. If we evaluate

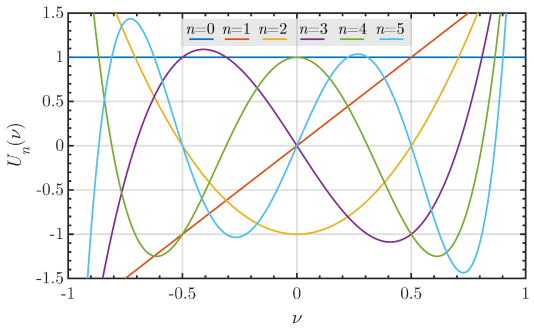

FIGURE B1. Modulus of the Tschebysheff polynomials of the second kind of order $n = 0, 1, \ldots, 5$.

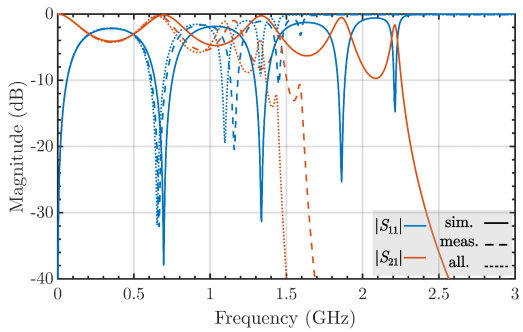

FIGURE C1. $|S_{11}|$ and $|S_{21}|$ as a function of frequency for a periodic structure with $n = 5$ and $d = \lambda/12$ at $f = 3$ GHz with $\epsilon_r = 4.7$, under different simulation scenarios: (i) Taking parasitic elements and ground vias into account (solid lines); (ii) taking only parasitic elements into account (dashed lines); (iii) neglecting both effects (dotted lines). The theoretically expected position of the transmission peaks based on the ideal scenario are shown with grey vertical lines.

the recursive formula of the second kind Tschebysheff polynomials at $\nu = \nu_k^n$, we can derive by using this property:

$$\left|U_{n+1}\left(\nu = \nu_k^n\right)\right| = \left|U_{n-1}\left(\nu = \nu_k^n\right)\right| = 1 \forall k = \{[1, n] \in \mathbb{Z}\} \tag{19}$$

This is, the Tschebysheff polynomials of the second kind of order $n-1$ and $n+1$, are 1 in magnitude at the zeros of the Tschebysheff polynomials of order n, namely $|U_{n+1}(\nu = \nu_k^n)| = |U_{n-1}(\nu = \nu_k^n)| = 1$, while $|U_n(\nu = \nu_k^n)| = 0$. This can be observed in Fig. B1, where $|U_n(\nu)|$ versus ν is shown. For example, at the zero of $|U_2|$, i.e., $|U_2(\nu = 0.5)| = 0$, we can observe that $|U_1(\nu = 0.5)| = 1$ and $|U_3(\nu = 0.5)| = 1$.

APPENDIX C
PARASITICS EFFECT

For a deeper understanding of the considerable impact that the packaging and the ground vias has on the circuit performance, Fig. C1 shows a comparison between the outcome of three different situations: (i) the equivalent circuit shown in Fig. 10 (dotted lines); (ii) the circuit without considering the ground vias elements (dashed lines); (iii) the circuit without considering the ground vias nor the parasitic elements (solid lines). It can be observed the great impact that these two factors due to the technology used for our demonstrator have on the final evolution of the parameters, shifting considerably the position of the transmission peaks along the frequency axis, as well as changing their magnitude and distance. It can be thus concluded that parasitics must be included for a proper circuit design.

ACKNOWLEDGMENT

The authors would like to express their gratitude to Mario Alberto Fernández Pantoja and to Carmen Torres Montijano for the fruitful discussions.

REFERENCES

[1] L. Brillouin, *Wave Propagation in Periodic Structures: Electric Filters and Crystal Lattices*, vol. 2. New York, NY, USA: Dover, 1953.
[2] Y. V. Serdyuk, A. D. Podoltsev, and S. M. Gubanski, "Numerical simulations of dielectric properties of composite material with periodic structure," *J. Electrostatics*, vol. 63, no. 11, pp. 1073–1091, 2005.
[3] S. Longhi, "Classical simulation of relativistic quantum mechanics in periodic optical structures," *Appl. Phys. B*, vol. 104, no. 3, pp. 453–468, 2011.
[4] R. E. Collin, *Foundations for Microwave Engineering*. Hoboken, NJ, USA: Wiley, 2007.
[5] D. M. Pozar, *Microwave Engineering*. Hoboken, NJ, USA: Wiley, 2011.
[6] J. Malherbe, *Microwave Transmission Line Filters*. Dedham, MA, USA: Artech House, 1979.
[7] I. Hunter, *Theory and Design of Microwave Filters*, vol. 48. London, U.K.: IET, 2001.
[8] H. A. Atwater, "Circuit design of the loaded-line phase shifter," *IEEE Trans. Microw. Theory Techn.*, vol. 33, no. 7, pp. 626–634, Jul. 1985.
[9] A. S. Nagra and R. A. York, "Distributed analog phase shifters with low insertion loss," *IEEE Trans. Microw. Theory Techn.*, vol. 47, no. 9, pp. 1705–1711, Sep. 1999.
[10] F. Ellinger, H. Jackel, and W. Bachtold, "Varactor-loaded transmission-line phase shifter at C-band using lumped elements," *IEEE Trans. Microw. Theory Techn.*, vol. 51, no. 4, pp. 1135–1140, Apr. 2003.
[11] H. Kim, A. B. Kozyrev, A. Karbassi, and D. V. D. Weide, "Linear tunable phase shifter using a left-handed transmission line," *IEEE Microw. Wireless Compon. Lett.*, vol. 15, no. 5, pp. 366–368, May 2005.
[12] Y.-H. Chun and J.-S. Hong, "A novel tunable transmission line and its application to a phase shifter," *IEEE Microw. Wireless Compon. Lett.*, vol. 15, no. 11, pp. 784–786, Nov. 2005.
[13] F. Lin and H. Deng, "Continuously tunable true-time-delay phase shifter based on transmission lines with simultaneously reconfigurable impedance and phase constant," *IEEE Trans. Microw. Theory Techn.*, vol. 67, no. 12, pp. 4714–4723, Dec. 2019.
[14] M. Yasir, S. Bistarelli, A. Cataldo, M. Bozzi, L. Perregrini, and S. Bellucci, "Tunable phase shifter based on few-layer graphene flakes," *IEEE Microw. Wireless Compon. Lett.*, vol. 29, no. 1, pp. 47–49, Jan. 2019.
[15] H. Ren, M. Zhou, Y. Gu, and B. Arigong, "A tunable transmission line with controllable phase shifting and characteristic impedance," *IEEE Trans. Circuits Syst. II, Exp. Briefs*, vol. 67, no. 10, pp. 1720–1724, Oct. 2020.
[16] R. Johnson, "Cascaded active twoports," *IRE Trans. Circuit Theory*, vol. 9, no. 1, pp. 33–37, Mar. 1962.
[17] B. Dasher and M. Moad, "Analysis of four-terminal cascade networks," *IEEE Trans. Circuit Theory*, vol. 11, no. 2, pp. 260–267, Jun. 1964.
[18] M. Pease, "The iterated network and its application to diifferentiators," *Proc. IRE*, vol. 40, no. 6, pp. 709–711, Jun. 1952.
[19] J. Perini, "Periodically loaded transmission lines," *IEEE Trans. Microw. Theory Techn.*, vol. 28, no. 9, pp. 1029–1031, Sep. 1980.
[20] D. J. Griffiths and C. A. Steinke, "Waves in locally periodic media," *Amer. J. Phys.*, vol. 69, no. 2, pp. 137–154, 2001.
[21] M. Abramowitz and I. A. Stegun, *Handbook of Mathematical Functions With Formulas, Graphs, and Mathematical Tables*, vol. 55. Washington DC, USA: U.S. Government Printing Office, 1964.
[22] "PDF files for ADS documentation," Keysight, Santa Rosa, CA, USA. Accessed: Oct. 04, 2022. [Online]. Available: https://edadocs.software.keysight.com/display/ads201101/PDF+Files+for+ADS+documentation

[23] "Placa de cobre para PCB, AD16, simple cara, base FR4, FR4, grosor 35µm, 100 × 160 × 1.6mm," Data Sheet, RS, Madrid, Spain. Accessed: Oct. 06, 2022.
[24] "Voltera conductor 2 (1000388)," Data Sheet, Voltera, Kitchener, ON, Canada. Accessed: Oct. 06, 2022.
[25] "BBY55series," Data Sheet, Infineon Technologies AG, München, Germany. Accessed: Oct. 05, 2022.
[26] "PG-SC79-2-1," Data Sheet, Infineon Technologies AG, München, Germany. Accessed: Oct. 06, 2022.
[27] M. E. Goldfarb and R. A. Pucel, "Modeling via hole grounds in microstrip," *IEEE Microw. Guided Wave Lett.*, vol. 1, no. 6, pp. 135–137, Jun. 1991.

ALBERTO MEDINA-RULL (Student Member, IEEE) received the M.S. degree in telecommunications engineering from the University of Granada, Granada, Spain, in 2020. He is currently working toward the Ph.D. degree. His research focuses on high frequency applications with 2D-material-based devices.

FRANCISCO PASADAS received the Ph.D. degree in electronic and telecommunication engineering from the Universitat Autónoma de Barcelona (UAB), Bellaterra, Spain, in 2017. From 2017 to 2021, he was a Postodoctoral Research with the Departament d'Enginyeria Electrònica, UAB, where he carried out the development of physics-based models of devices based on graphene and related materials. He is currently with the Departamento de Electrónica y Tecnología de Computadores, Universidad de Granada, Granada, Spain. His research interests include the modeling of flexible 2D devices and the design of novel radio-frequency applications based on emergent 2D technologies.

ENRIQUE G. MARIN received the Ph.D. degree in electronics from the University of Granada, Granada, Spain, in 2014. He has carried out his research career with IBM Research Zurich, Switzerland; Cornell University, Ithaca, NY, USA; and the University of Pisa, Pisa, Italy. He is currently with the Departament of Electronics, University of Granada, Granada, Spain.

ANDRÉS GODOY received the M.S. and Ph.D. degrees in physics from the University of Granada, Granada, Spain. Since 2011, he has been a Professor with the Department of Electronics, University of Granada.

FRANCISCO G. RUIZ (Member, IEEE) received the telecommunication engineering degree from the University of Málaga, Málaga, Spain, in 2002, and the Ph.D. degree in physics from the University of Granada, Granada, Spain, in 2005. Since 2006, he has been with the Department of Electronics, University of Granada, where he co-founded the Pervasive Electronics Advanced Research Laboratory in 2018. He was a Visiting Researcher with TUDelft, UCL, IMEC, and Universitaet Siegen. His research interests include 2D materials based electron devices, including RF devices and circuits, sensors, optoelectronic devices and neuromorphic devices, and circuits.